Sun et al. *NPG Asia Materials* (2021) 13:21
https://doi.org/10.1038/s41427-020-00252-1

NPG Asia Materials

ARTICLE Open Access

Selective reaction of conjugated polymers with basic proteins for broad-spectrum antivirulence therapy

Han Sun[1,2], Jing Liu[3], Fengting Lv[1], Libing Liu[1,2], Qi Gu[3], Baoyang Hu[3] and Shu Wang[1,2]

Abstract

Antivirulence therapy has proven to be an attractive method for the treatment of bacterial infections and venomous injuries; however, the approaches for neutralizing multiple types of virulence through one platform are limited. To address this challenge, we have developed a reactive conjugated polymer, PPV–NHS, which functions as a broad-spectrum antidote for directly inactivating basic toxins. The antivirulence is achieved via multivalent electrostatic recognition and subsequent amidation reactions between PPV–NHS and toxins. The resultant bioconjugates significantly reduced neurotoxicity and cytotoxicity. In the mouse model, PPV–NHS effectively inhibited the toxicity of cardiotoxin (CTX) and improved the survival rate of toxin-challenged mice. This work represents the rational design of functionalized conjugated polymers for antivirulence therapy with both high efficiency and broad applicability.

Introduction

Millions of lives are taken away each year due to the pathogenicity caused by biotoxins. Proteins and peptides from microorganism infections and venomous injuries are the main pathogenic causes[1–3]. Toxin-targeted antivirulence therapy has proven to be an attractive method for the treatment of these diseases[4,5]. Antisera[6], antibodies[7], and vaccines[8] are common methods to eliminate toxins. Nevertheless, these treatments only target-specific pathogens. Moreover, the shortage of antivenoms has become a global problem due to their high storage cost and long development period[9]. In recent years, some small molecules[10], polymers[11,12], and nanomaterials[13,14] have also been used for detoxification by binding to specific targets of toxins. However, the development of a broad-spectrum detox platform remains limited and urgent, especially for emergencies where poisonous bite and pathogen subtypes cannot be identified and diagnosed in time.

Through the analyses of the structures and properties of a large number of toxins, we found that many common toxins are basic proteins. For example, all 50 determined postsynaptic neurotoxins from snake venoms are basic proteins with isoelectric points (pIs) in the range of 9–10[15], and α-hemolysin, γ-hemolysin, and leucocidin of different staphylococcal strains show similarities with isoelectric points of 7.3–9.5[16]. A family of homologous toxins from scorpion venoms that affect Na-channel and K-channel functions are basic peptides[17,18]. In addition, many viruses also have positively charged envelope and capsid proteins[19–21]. The positive charges on the surface of basic toxins play important roles both in damaging plasma membrane and binding membrane receptors through electrostatic interactions with negatively charged phospholipids and acidic domains of receptors. Thus, the development of materials that recognize and inactive basic protein toxins offers great potential for

Correspondence: Baoyang Hu (byhu@ioz.ac.cn) or Shu Wang (wangshu@iccas.ac.cn)
[1]Beijing National Laboratory for Molecular Sciences, Key Laboratory of Organic Solids, Institute of Chemistry, Chinese Academy of Sciences, 100910 Beijing, P.R. China
[2]College of Chemistry, University of Chinese Academy of Sciences, 100049 Beijing, P.R. China
Full list of author information is available at the end of the article

broad-spectrum detoxification treatment. Renner et al. synthesized polymeric bisphosphonate hosts with high affinities for basic proteins, which provides a foundation to recognize basic toxins through multivalent electrostatic interactions[22]. In addition, covalent inhibitors display increased potency and prolonged activity over non-covalent analogs. Therefore, designing a process of initial recognition and then the covalent reaction may be useful for antivirulence therapy.

We designed a series of reactive conjugated polymers that can be attached to different amyloid proteins[23,24]. The anionic poly(*p*-phenylene vinylene) functionalized with carbocyclic acid and N-hydroxysuccinimide ester (PPV–NHS) can react with positively charged islet amyloid polypeptide (IAPP) through amidation reactions, which effectively inhibits the cytotoxicity of the IAPP. In this work, we systematically investigated the interactions of PPV–NHS with different kinds of biomolecules. The results showed that PPV–NHS selectively binds to basic proteins through electrostatic recognition then covalent interactions (Scheme 1a). PPV–NHS was subsequently used for the detoxification of α-bungarotoxin (α-BTX) and cardiotoxin (CTX), demonstrating excellent inhibitory effects on neurotoxicity and hemolysis in vitro and in vivo (Scheme 1b). In addition, the fluorescent property of the PPV–NHS backbone is also used to track its distribution and metabolism in vivo. PPV–NHS has great potential as a broad-spectrum detoxification platform for antivirulence therapy.

Materials and methods

Materials

All organic solvents were purchased from Beijing Chemical Works. Organic reagents were purchased from Acros, Sigma-Aldrich, and Alfa-Aesar. Proteins were purchased from Sigma-Aldrich. PPE–NHS was synthesized by two-step esterification of a precursor polymer, poly(*p*-phenylene vinylene), which contains hydroxyl groups (PPV–OH) according to the literature[23]. The number average molecular weight of PPV–OH is 25000 with a polydispersity of 1.15. The number average degree of polymerization is 18. Chemicals for SDS-PAGE and tricine-SDS-PAGE were purchased from Solarbio. A peroxidase assay kit was purchased from Thermo Fisher. α-BTX, crotamine, and CTX were purchased from Guangzhou Whiga Technology, Ltd. The PC12 cell line was purchased from the cell culture center of the Institute of Basic Medical Sciences, Chinese Academy of Medical Sciences (Beijing, China). Fresh mouse blood samples and mice were kindly supplied by the Institute of Zoology, Chinese Academy of Sciences. Human blood samples were obtained from Sanbo Brain Hospital, Capital Medical University (Beijing, P. R. China). These samples were from patients without blood disease prior to any treatment. Informed consent was obtained from all patients prior to the study. C57BL/6 mice were used as healthy mice for animal experiments.

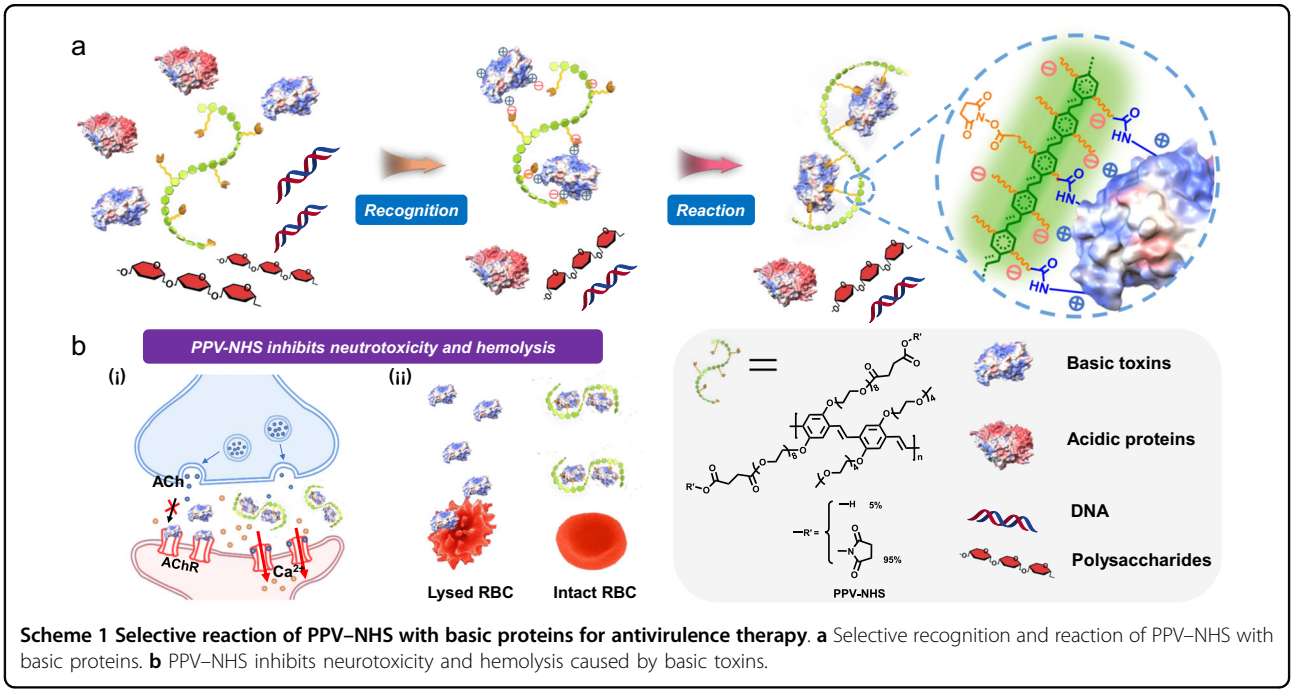

Scheme 1 Selective reaction of PPV–NHS with basic proteins for antivirulence therapy. **a** Selective recognition and reaction of PPV–NHS with basic proteins. **b** PPV–NHS inhibits neurotoxicity and hemolysis caused by basic toxins.

Apparatus

The ^{1}H NMR spectra were recorded on a Bruker AVANCE 300-MHz spectrometer. The absolute fluorescence quantum yield was recorded on a Hamamatsu absolute PL C11347 series quantum yield spectrometer. Gel electrophoresis experiments were performed with a Mini-PROTEIN Tetra System from Bio-Rad. Gel photographs were taken with a Bio-Rad Molecular Imager ChemiDoc XRS system. Zeta potentials and hydration sphere diameters were measured on a Nano ZS (ZEN3600) system. Fluorescence images were taken with a confocal laser-scanning microscope (FV1000-IX81, Olympus, Japan). UV–vis absorption spectra were measured on a JASCO V-550 spectrophotometer. Fluorescence spectra were recorded on a Hitachi F-4500 fluorometer with a xenon lamp excitation source or a Varioskan Flash (Thermo Scientific Company, USA). SEM images were captured using a Hitachi S-4800 scanning electron microscope. Biodistribution of PPV–NHS in mice was performed with an IVIS® spectrum imaging system (Caliper Life Sciences, USA).

Gel electrophoresis

Sodium dodecyl sulfate-polyacrylamide gel electrophoresis (SDS-PAGE) and tricine-SDS-PAGE were performed to investigate the selective reaction of PPV–NHS with different proteins. Proteins (20 μM) were incubated with PPV–NHS in 10 mM PBS at 37 °C for 30 min at molar concentration ratios of 1:1, 1:5, 1:10, and 1:20. Proteins including HRP, BOD, GOD, BSA, G6PD, and LPO were denatured in 2 × SDS-PAGE loading buffer at 90 °C for 10 min. After cooling to room temperature, the samples were loaded in a vertical SDS-PAGE system with 12% separating and 5% stacking layers. SDS-PAGE was run on gels in running buffer (250 mM glycine, 25 mM Tris Base, and 0.1% SDS, pH 8.3) for 60 min at 200 V. As low-molecular-weight proteins, α-CT, Pap, Cyt c, Lys, and CTX were denatured in 2× Tris-Tricine-SDS-PAGE loading buffer at 90 °C for 10 min. The proteins and protein–polymer complexes were loaded in a vertical tricine-SDS-PAGE system with 16.5% separating, 10% intermediate, and 4% stacking layers. Anode buffer and cathode buffer were added to the external and internal electrophoresis tanks, respectively. Gels were run for 60 min at 30 V, followed by 60 min at 100 V. The resultant gels were washed with dd-H_2O and stained with Coomassie brilliant blue.

Zeta potential and DLS measurements

BSA, GOD, HRP, α-CT, and Cyt c (10 μM) were mixed with PPV–NHS (10 μM) in 1 mL of water. Then, the solutions were used for zeta potential and DLS measurements. Untreated PPV–NHS (10 μM) was employed as a control.

Measurement of the catalytic activity of the proteins

HRP and LPO are two kinds of peroxidases with opposite surface charges. The impact of PPV–NHS on enzyme activity was measured. PPV–NHS (200 μM) and HRP (20 μM) were incubated at 37 °C for 30 min. The solution was diluted 100,000-fold with PBS. The Amplex® red reagent (10-acetyl-3,7-dihydroxyphenoxazine) was used to detect peroxidase activity. The fluorescence intensities of oxidized Amplex® red reagent at 590 nm were recorded with time. The excitation wavelength was 565 nm. The slope of the linear regression of the linear portion of the fluorescence over time was used to measure the protein activity. The apparent activity was calculated relative to the protein alone. For LPO, a similar procedure was employed except that the sample was diluted 500-fold with PBS to ensure that the values aligned with the linear part of the fluorescence intensities as a function of the enzyme concentrations.

Cell assay for Ca^{2+} influx

PC12 cells were cultured in RPMI 1640 medium containing 10% fetal bovine serum under 5% CO_2 at 37 °C. The cells were washed with PBS and treated with PPV–NHS (2.5 μM), α-BTX (0.5 μM), and PPV–NHS (2.5 μM)/α-BTX (0.5 μM) mixtures in RPMI 1640 medium for 1 h. Cells cultured with only RPMI 1640 medium were used as a control. Then, the cells were washed with PBS three times and stained with Fluo-8 (5 μM) in MEM (without $CaCl_2$) for 30 min. Then, the cells were washed with PBS three times and treated with MEM containing 200 mg/L $CaCl_2$ and 500 μM ACh. The cells were observed with confocal laser-scanning microscopy using a 488-nm laser.

Hemolytic assays

The ability of PPV–NHS to inhibit CTX toxicity was investigated by hemolytic assays. Specifically, red blood cells (RBCs) were collected into heparinized tubes and washed two times by gentle resuspension with 10 mM PBS. The RBCs were centrifuged at 1500 RCF for 10 min at 4 °C and diluted to 2% (v/v). A mixture of CTX (10 μM) and RBCs in PBS was incubated with PPV–NHS (50 μM) for 8 h at 37 °C. The absorbance of hemoglobin at 576 nm was recorded at 1-h intervals after the RBCs were pelleted by centrifugation (1500 RCF, 10 min). The group with only PBS added was set as the negative control, and 1% Triton-X 100 was added as the positive control.

$$\text{The \% hemolysis} = \frac{\text{A576 of RBCs treated with sample} - \text{A576 of RBCs in PBS}}{\text{A576 of RBCs treated with triton X 100} - \text{A576 of RBCs in PBS}} \times 100$$

SEM measurements

SEM characterization was employed to directly visualize the morphological changes of the RBCs treated with CTX

and PPV–NHS. After the procedure used in the hemolytic assays, the pellets were fixed overnight with 1 mL of 2.5% glutaraldehyde in PBS at 4 °C. Then, 10 μL aliquots of RBC suspensions were transferred onto clean silicon slices and dried. After drying, 0.1% glutaraldehyde was added and incubated for 3 h for further fixation. Then, the specimens were washed with sterile water twice and dehydrated with increasing concentrations of ethanol (70% for 6 min, 90% for 6 min, and 100% for 6 min). Finally, the dried specimens were coated with platinum for SEM measurements.

Detoxification in mice

To investigate the detoxification effect of PPV–NHS against CTX in vivo, healthy mice (weighing 18–22 g) were used for relevant tests. Seven mice were treated with CTX (25 μM, 200 μL) by intravenous injection into the tail vein. Seven mice were treated with PPV–NHS (125 μM, 200 μL). Seven mice were first injected with CTX (25 μM, 200 μL), and 3 min later, they were injected with PPV–NHS (125 μM, 200 μL). The survival time of the mice was recorded. Both CTX and PPV–NHS were dissolved in 10 mM PBS.

Results

Selective reaction of PPV–NHS

Ten proteins, horseradish peroxidase (HRP), bilirubin oxidase (BOD), glucose oxidase (GOD), bovine serum albumin (BSA), glucose-6-phosphate dehydrogenase (G6PD), α-chymotrypsin (α-CT), papain (Pap), lactoperoxidase (LPO), cytochrome c (Cyt c), and lysozyme (Lys), were employed to investigate the reaction selectivity of PPV–NHS. The basic properties of these proteins are listed in Supplementary Table S1. These proteins were incubated with PPV–NHS at molar concentration (repeat unit for PPV–NHS) ratios of 1:1, 1:5, 1:10, and 1:20 at 37 °C for 30 min. Denaturing polyacrylamide gel electrophoresis (SDS-PAGE) was used to characterize the extent of the protein covalent reaction with PPV–NHS. As shown in Fig. 1, proteins with isoelectric points (pIs) lower than 7.4 did not exhibit changed molecular weights in the gel after incubation with PPV–NHS, indicating that the coupling reaction was prohibited. HRP, BOD, GOD, and G6PD did not react with PPV–NHS even when PPV–NHS was present in excess of 20-fold. Only the bands of BSA decreased slightly with increasing concentrations of PPV–NHS. In contrast, proteins with pI

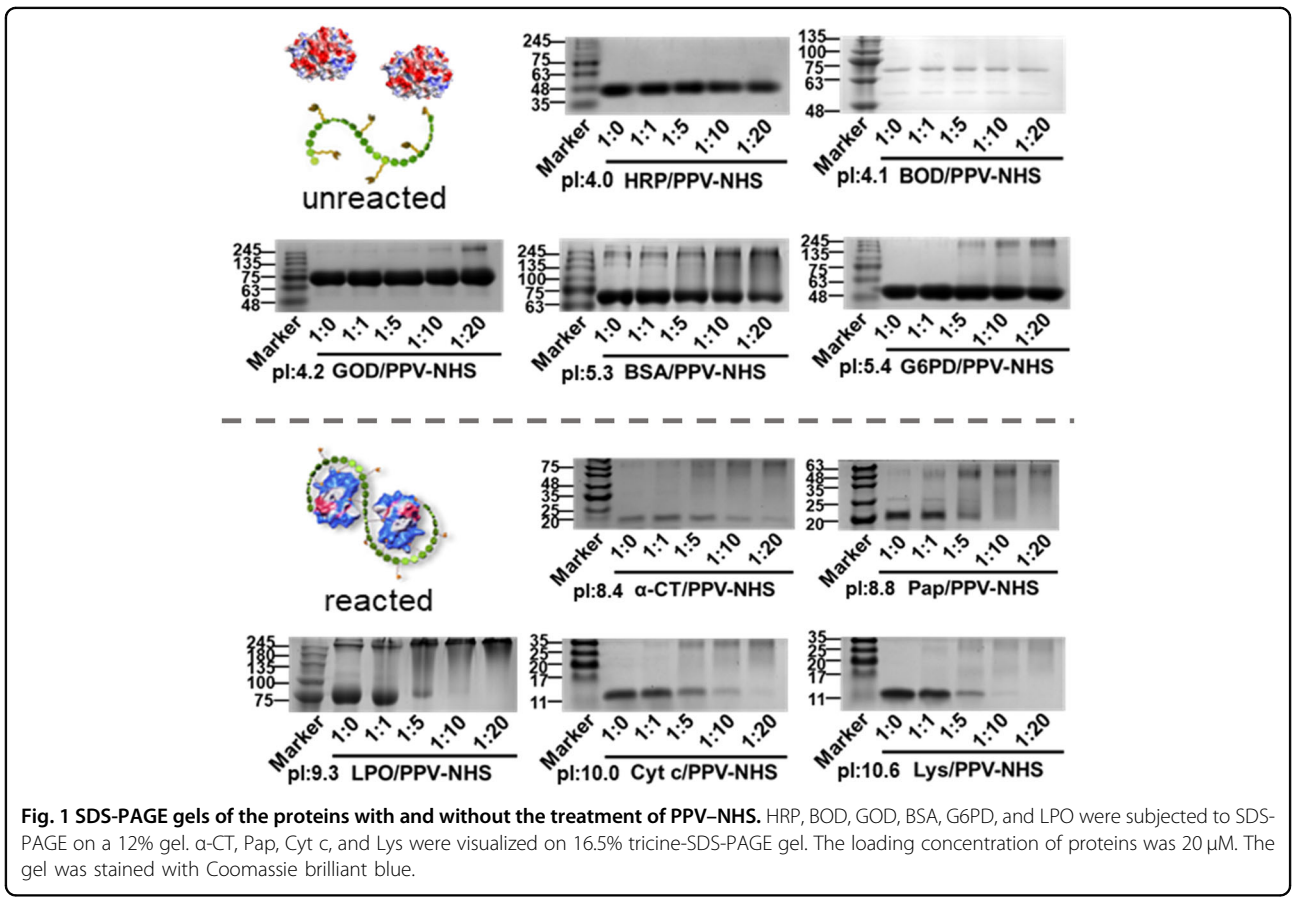

Fig. 1 SDS-PAGE gels of the proteins with and without the treatment of PPV–NHS. HRP, BOD, GOD, BSA, G6PD, and LPO were subjected to SDS-PAGE on a 12% gel. α-CT, Pap, Cyt c, and Lys were visualized on 16.5% tricine-SDS-PAGE gel. The loading concentration of proteins was 20 μM. The gel was stained with Coomassie brilliant blue.

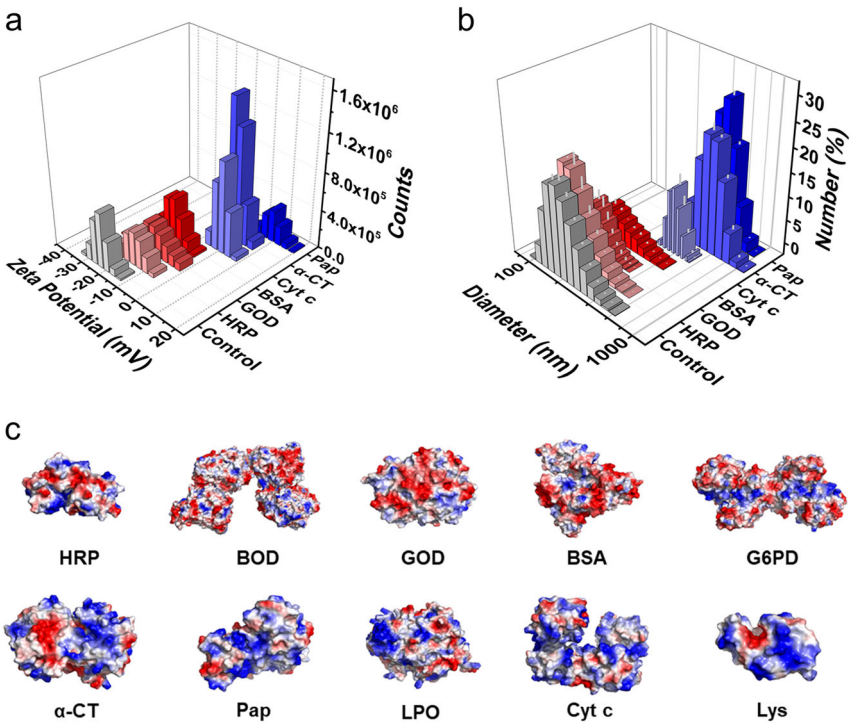

Fig. 2 Electrostatic recognition between basic proteins and PPV–NHS. Zeta potentials (**a**) and hydrodynamic diameters (**b**) of PPV–NHS (10 μM) in the absence and presence of acidic proteins (HRP, GOD, and BSA) (10 μM) and basic proteins (Cyt c, α-CT, and Pap) (10 μM). **c** Connolly surface was patterned with ESP to show the distribution of protein surface charges, which were colored in red (acidic domains) and blue (basic domains).

values above 7.4 exhibited good reactivity. The monomer bands of Pap, LPO, Cyt c, and Lys decreased significantly after incubation with PPV–NHS in fivefold excess. All proteins were converted to protein–polymer conjugates when PPV–NHS was in excess of 20-fold. These results demonstrated that PPV–NHS could selectively react with basic proteins in a dose-dependent manner. We also investigated the reaction of PPV–NHS with other biomolecules, such as DNA and polysaccharides. The agarose electrophoresis results showed that they could not react with PPV–NHS (Supplementary Fig. S1).

The mechanism of the selective reactivity of PPV–NHS

To study the mechanism of the selective reactivity of PPV–NHS towards basic proteins, zeta (ζ) potential was used to measure the surface charge changes of PPV–NHS after conjugation with proteins. Figure 2a summarizes the potential of PPV–NHS in the absence and presence of proteins with different pI values. PPV–NHS is negatively charged with a ζ potential of -21.1 ± 0.1 mV. After incubation with BSA, GOD, and HRP, the surface charge of PPV–NHS did not change. In contrast, in the presence of positively charged proteins (Pap, α-CT, and Cyt c), the ζ potential of PPV–NHS shifted from negative to positive values. These results indicated that PPV–NHS attached to basic proteins through electrostatic interactions. Dynamic light-scattering (DLS) data revealed a significantly increased hydration sphere diameter of PPV–NHS in the presence of basic proteins, but when PPV–NHS was treated with acidic proteins, the PPV–NHS diameter was negligibly changed (Fig. 2b). The DLS and ζ potential results are consistent with the SDS-PAGE experiment, indicating the electrostatic recognition and reaction between PPV–NHS and basic proteins.

A closer inspection of the surface charge distribution of proteins provided further insight into factors that influence the bioconjugation process. For this purpose, the electrostatic surface potential (ESP) of the proteins was calculated. The crystal structures of the proteins were obtained from the RCSB PDB. The Connolly surface was colored in red (acidic domains) and blue (basic domains) to display the ESP of proteins. As shown in Fig. 2c, the surfaces of HRP, BOD, GOD, BSA, and G6PD showed a high density of negative charges, which was unfavorable for PPV–NHS binding. In contrast, α-CT, Pap, LPO, Cyt c, and Lys were uniformly covered with basic residues, which facilitated their high affinity for PPV–NHS. To further confirm the effect of the protein surface charge on the bioconjugation reaction, the reactions were performed under high-salt concentrations to destroy the electrostatic interactions. Compared with treatment in 0.01 M phosphate-buffered saline (PBS), the reaction of

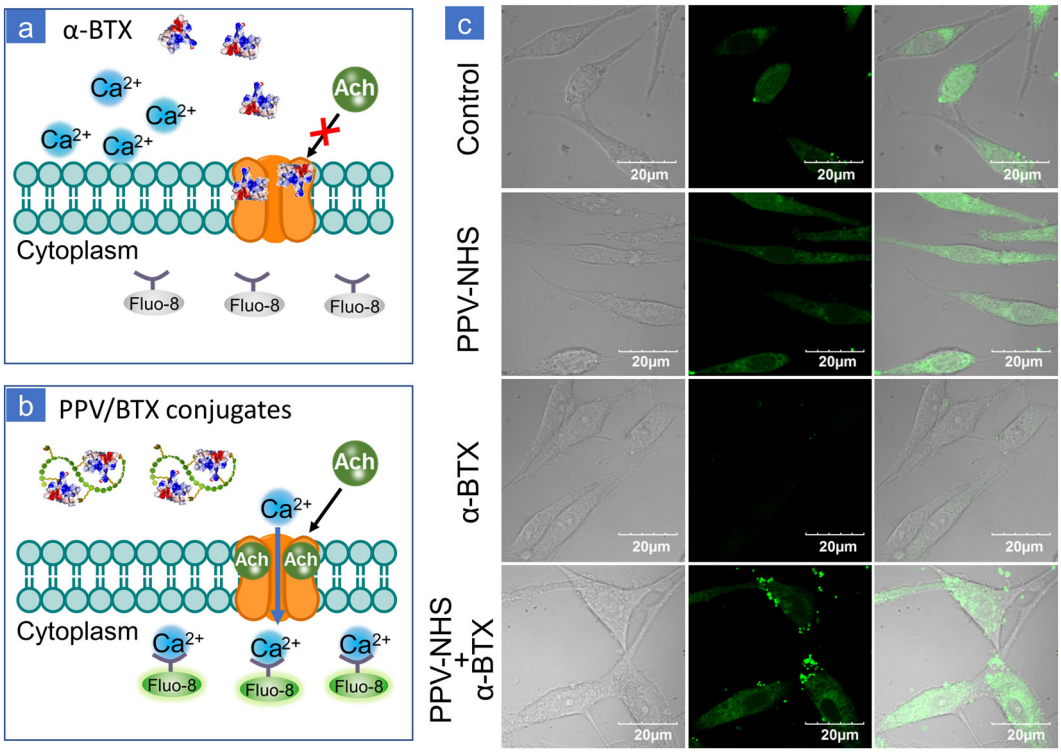

Fig. 3 Detoxication of α-BTX by PPV–NHS. a Schematic illustration of α-BTX competitively binding to nAChRs and blocking the ion channel. **b** Schematic illustration of the detoxication effect of PPV–NHS on α-BTX. The intracellular Ca^{2+} indicator Fluo-8 was turned on, i.e., fluoresced, due to the opening of ligand-gated the nAChR channels. **c** CLSM images of PC12 cells after the treatment with PPV–NHS (2.5 μM), α-BTX (0.5 μM), and PPV–NHS (2.5 μM)/α-BTX (0.5 μM) complexes. Left: phase-contrast bright-field image. Middle: fluorescence image. Right: merged image.

PPV–NHS with proteins in 0.2 M and 0.5 M PBS was suppressed (Supplementary Fig. S2). As the ionic strength of the medium increased, the degree of reaction decreased. These results demonstrate that the electrostatic recognition between basic proteins and PPV–NHS is critical for the bioconjugation reaction. Although acidic proteins show many reactive lysine residues (Supplementary Table S1), they cannot react with PPV–NHS under physiological conditions due to electrostatic repulsion. We next investigated the effect of PPV–NHS on protein function. HRP and LPO are both peroxidases but possess opposite surface charges. As shown in Supplementary Fig. S3, the activity of HRP did not change in the presence of PPV–NHS. In contrast, when PPV–NHS was added to an LPO solution, the activity was inhibited to ~60%. We speculate that PPV–NHS selectively inhibits basic protein activity through multivalent interactions that change protein structure and block catalytic active sites.

Detoxification of basic toxins

To investigate the ability of PPV–NHS to detoxify basic toxins, three kinds of toxins (α-BTX, crotamine, and CTX) from different snake venoms were used to interact with PPV–NHS. The ESP calculation of these toxins displayed a high density of positive charges on the surface, which showed high reactivity to PPV–NHS (Supplementary Fig. S4a). When PPV–NHS was in tenfold excess, these toxins were totally converted into PPV–toxin conjugates through amidation reactions, as indicated with tricine-SDS-PAGE gel analysis (Supplementary Fig. S4b). We further investigated whether PPV–NHS can neutralize the toxicity of α-BTX and CTX in vitro and in vivo. α-BTX can competitively and irreversibly bind to nicotinic acetylcholine receptors (nAChRs) in the vertebrate nervous system. nAChRs are cation-selective ligand-gated ion channels with a high permeability of calcium. The binding of α-BTX inhibits nAChR function, causing paralysis, respiratory failure, and death in patients. The rat pheochromocytoma cell line (PC12) expresses multiple nAChRs and was used as a model cell for studying the detoxification effect of PPV–NHS on α-BTX. Calcium influx was detected by the indicator Fluo-8, which is turned "on" in the presence of intracellular calcium. The intracellular fluorescence was monitored by confocal laser-scanning

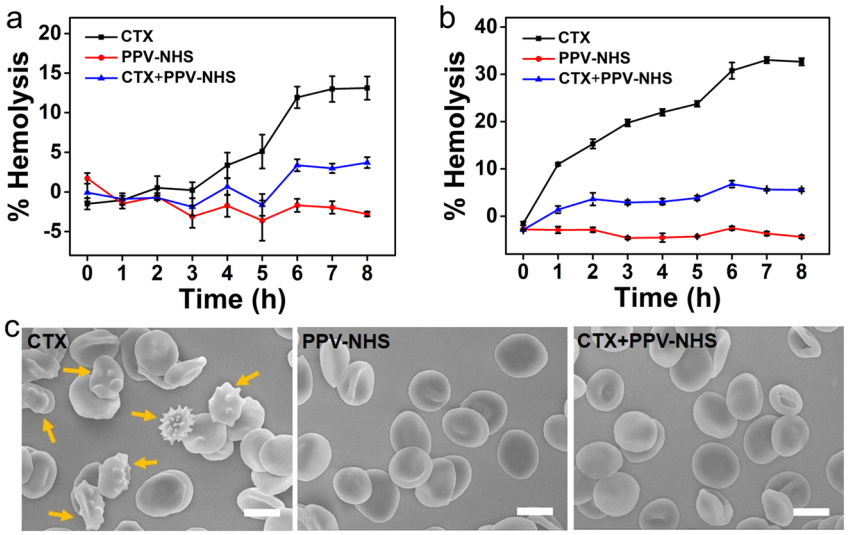

Fig. 4 PPV–NHS inhibited the hemolytic activity of CTX. Time course of hemolysis induced by CTX (10 μM) with and without PPV–NHS (50 μM) in mouse (**a**) and human (**b**) blood. **c** Morphology of human red blood cells (RBCs) treated with CTX in the absence and presence of PPV–NHS. Arrows indicate acanthocytes and membrane blebbing of RBCs. The scale bars are 5 μm.

microscopy (CLSM). As shown in the control group of Fig. 3c, with the treatment of only acetylcholine (ACh) to PC12 cells, a significant fluorescence signal was observed, demonstrating calcium influx through the binding of ACh to nAChRs. The cells pretreated with PPV–NHS also exhibited high fluorescence intensity, indicating that PPV–NHS cannot influence the binding process (Fig. 3c). As expected, cells pretreated with α-BTX did not show an increase in fluorescence intensity after ACh was added (Fig. 3c) because α-BTX competitively blocks nAChR from accessing the Ach-binding sites, which prevents calcium transfer into cells. In contrast, upon treatment of with the PPV–NHS/α-BTX complex, PC12 cells in ACh solution displayed a highly intense fluorescence signal, which was similar to that of the control group (Fig. 3c), indicating that PPV–NHS effectively prevented the blocking effect of α-BTX on nAChR. Therefore, PPV–NHS can inhibit the neurotoxicity of α-BTX in the neuromuscular junction.

CTX can disrupt the matrix of the cell membrane organization, causing lysis of RBCs. The detoxification effect of PPV–NHS on CTX was determined by hemolysis assays. As shown in Fig. 4a, b, the addition of CTX to the suspension of RBCs induced the obvious release of hemoglobin. Human RBCs are more susceptible to CTX than mouse RBCs. In the presence of PPV–NHS, the RBC rupture by CTX was inhibited, and PPV–NHS did not cause visible destruction to the RBCs. The morphological changes of the RBCs under different treatments were observed by scanning electron microscopy (SEM). RBCs in PBS displayed the typical discocyte shape (Supplementary Fig. S5). After the addition of CTX, the RBCs changed into acanthocytes, and membrane blebbing was observed (Fig. 4c). RBCs treated with PPV–NHS maintained their discocyte shape in the presence of CTX, indicating that the formation of the PPV–CTX assemblies inhibited the hemolytic activity of CTX. The hemolytic kinetics assay and SEM images demonstrated the effective inactivation of CTX by PPV–NHS.

Animal experiments were also conducted to explore whether PPV–NHS can neutralize the toxicity of CTX in vivo (Fig. 5a). Notably, most of the proteins in blood are negatively charged with low pI values[25,26]. Thus, their activity was not expected to be affected by PPV–NHS. After intravenous injection of CTX (25 μM, 200 μL), all mice died within 18 min (Fig. 5b). Fifty-seven percent of the mice survived when injected with PPV–NHS (125 μM, 200 μL) after injection of CTX (Fig. 5b). Although 43% of the mice died, the survival time of these mice was extended to ~50 min. Conjugated polymers have been widely used in the bioimaging field because of their excellent light-harvesting ability, optical stability, and high fluorescence quantum yield[27–29]. The UV–vis absorption and emission spectra of PPV–NHS are shown in Supplementary Fig. S6. PPV–NHS displayed a maximum absorption peak at 450 nm and a maximum emission peak at 555 nm with an absolute fluorescence quantum yield of 16% in water. Therefore, the biodistribution of PPV–NHS with and without CTX was investigated in mice by measuring the fluorescence signal of PPV–NHS. The mice were sacrificed, and the

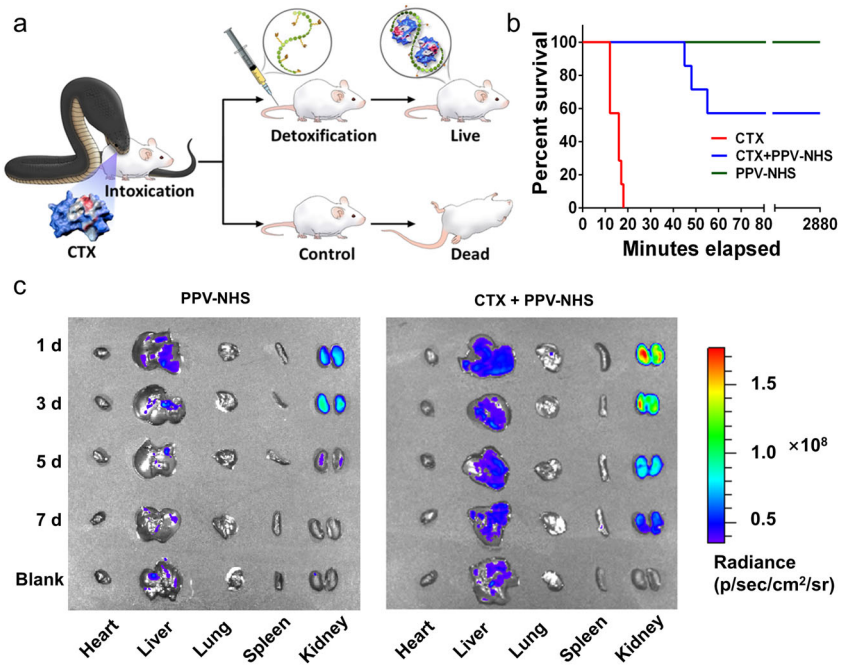

Fig. 5 Detoxication of CTX by PPV–NHS in vivo. a Schematic illustration of the detoxification of CTX by using PPV–NHS in vivo. **b** The percentage of mice that survived after intravenous injection of CTX (25 μM), PPV–NHS (125 μM), and successive injection of CTX and PPV–NHS, for which the interval time was 3 min. **c** Biodistribution of PPV–NHS (100 μM, 150 μL) in mouse organs without CTX and preinjected CTX (20 μM, 150 μL); the interval time of injection was 3 min. Fluorescence images were taken on days 1, 3, 5, and 7 by an IVIS® spectrum imaging system with an excitation wavelength of 465 nm and an emission wavelength of 540 nm.

organs, including the heart, liver, lung, spleen, and kidney, were harvested after intravenous injection of PPV–NHS and CTX followed by PPV–NHS. The fluorescence images and corresponding statistical results are displayed in Figs. 5c and Supplementary Fig. S7. PPV–NHS was mainly distributed in the kidney, and eliminated in 7 days. However, PPV–NHS injected after CTX exhibited prolonged retention time, suggesting that PPV–NHS reacted with CTX in vivo and formed complexes that caused its longer half-life. Combined with the aforementioned experiment, we concluded that PPV–NHS could inhibit the toxicity of CTX in vivo and is excreted over time.

Discussion

Toxin proteins can cause physical damage, biochemical degradation, and signaling interruption in mammals, leading to disabilities and even death. Antivirulence therapy is receiving increasing attention, especially because it does not directly kill bacteria, which may delay the development of bacterial resistance. However, most of the current antitoxins were developed against specific toxins, and broad-spectrum antitoxic platforms are rare. By analyzing their amino acid sequences, we found that many toxins are basic proteins. These representative toxins are listed in Table 1 and ranged from bacterial exotoxins, animal venom toxins, and marine toxins to plant toxins. Some viruses also exhibit positive charges on the surface, such as *poliovirus* and *rotavirus A*. The selective and irreversible binding to these toxins may change their structure and function, which may be an effective strategy to neutralize the toxicity of the biotoxins and achieve a broad-spectrum detoxification effect.

In this work, we studied the interactions of PPV–NHS with different proteins. PPV–NHS can selectively react with basic proteins through multivalent electrostatic recognition before amidation reactions. Peroxidase activity experiments showed that the formation of PPV–protein bioconjugates can reduce the activity of the proteins. Then, we used α-BTX and CTX as models to study the detoxification effects of PPV on their ability to induce neurotoxicity and hemolysis in vitro and in vivo. PPV–NHS effectively prevented the blocking of nAChRs by α-BTX, protected RBCs from CTX damage, and significantly improved the survival rate of toxin-challenged mice. Taking advantage of the high fluorescence quantum yield of PPV–NHS, we tracked the distribution and metabolism of PPV–NHS in mice using an IVIS spectrum imaging system. PPV–NHS can be excreted in a week, indicating the possibility that it has biodegradable

Table 1 An overview of basic virulence factors.

Toxins	Organism(s)	M.W. (KD)	pI[a]	Mode of action	References
α-Hemolysin	*Staphylococcus aureus*	33.25	7.94	Lyses a variety of mammalian cells	16,30
γ-Hemolysin	*Staphylococcus aureus*	31.81	9.52	Lyses leukocytes	16,31
Leukocidin	*Staphylococcus aureus*	32.39	8.77	Lyses leukocytes	16
Listeriolysin O	*Listeria monocytogenes*	54.19	7.90	Lyses phagosomes	32
Melittin	*Apis mellifera*	2.85	12.01	Anaphylaxis and hemolysis	33
Buthotoxin	*Tityus serrulatus, Tityus bahiensis, and Tityus stigmurus*	4.51	7.32	Blocks potassium channels and inhibits the proliferation of T-cells	34
Kurtoxin	*Parabuthus transvaalicus*	7.39	7.91	Affects sodium channels and calcium channels	18
Calciseptine	*Dendroaspis polylepis*	7.04	7.92	Blocks calcium channels	35
Calcicludine	*Dendroaspis angusticeps*	6.99	8.92	Blocks calcium channels	36
α-Cobratoxin	*Naja cobras*	7.83	7.36	Blocks muscle-type and neuronal type nAChRs	37
α-Bungarotoxin	*Bungarus multicinctus*	7.99	8.82	Blocks nAChRs at neuromuscular junctions	38
Crotamine	*Crotalus durissus terrificus*	4.89	9.93	Affects sodium channels and promotes necrosis	39
Cardiotoxin	*Naja naja*	6.64	10.03	Causes myofiber necrosis and hemolysis	40
Maurocalcine	*Scorpio palmatus*	3.86	9.79	Activates calcium releases channels	41
ω-Conotoxins CVID	*Conus magus*	2.74	9.11	Blocks calcium channels	42
Viscotoxin B	*Viscum album*	4.86	9.09	Disrupts membrane bilayer	43
Poliovirus	*Poliovirus, PV-1 Mahoney*		8.3[b]	Poliomyelitis	44
Rotavirus A	*Rotavirus A, Simian rotavirus A/SA11*		8.0[b]	Causes inflammation in the stomach and intestines	21

[a]The isoelectric points are calculated according to the reference[45].
[b]The isoelectric points of a virus are measured by isoelectric focusing, as reported by references[21,44].

properties. Overall, these results demonstrated the broad applicability and effectiveness of PPV–NHS as an anti-virulence platform against basic toxin proteins.

Acknowledgements
We thank the Strategic Priority Research Program of the Chinese Academy of Sciences (XDA16020804) and the National Natural Science Foundation of China (21533012 and 21661132006) for financial support.

Author details
[1]Beijing National Laboratory for Molecular Sciences, Key Laboratory of Organic Solids, Institute of Chemistry, Chinese Academy of Sciences, 100910 Beijing, P.R. China. [2]College of Chemistry, University of Chinese Academy of Sciences, 100049 Beijing, P.R. China. [3]Institute of Zoology, Chinese Academy of Sciences, 100101 Beijing, P.R. China

Conflict of interest
The authors declare that they have no conflict of interest.

Supplementary information is available for this paper at https://doi.org/10.1038/s41427-020-00252-1.

Received: 12 July 2020 Revised: 18 August 2020 Accepted: 2 September 2020.
Published online: 8 March 2021

References

1. Fleitas Martínez, O., Cardoso, M. H., Ribeiro, S. M. & Franco, O. L. Recent advances in anti-virulence therapeutic strategies with a focus on dismantling bacterial membrane microdomains, toxin neutralization, quorum-sensing interference and biofilm inhibition. *Front. Cell. Infect. Microbiol.* **9**, 74–74 (2019).
2. Utkin, Y. N. Three-finger toxins, a deadly weapon of elapid venom-milestones of discovery. *Toxicon* **62**, 50–55 (2013).
3. Ivarsson, M. E., Leroux, J.-C. & Castagner, B. Targeting bacterial toxins. *Angew. Chem. Int. Ed.* **51**, 4024–4045 (2012).
4. Allen, R. C., Popat, R., Diggle, S. P. & Brown, S. P. Targeting virulence: can we make evolution-proof drugs? *Nat. Rev. Microbiol.* **12**, 300–308 (2014).
5. Rasko, D. A. & Sperandio, V. Anti-virulence strategies to combat bacteria-mediated disease. *Nat. Rev. Drug Discov.* **9**, 117–128 (2010).
6. Bierdeman, M. A., Torres, A. M., Caballero, A. R., Tang, A. & O'Callaghan, R. J. Reactions with antisera and pathological effects of *Staphylococcus aureus* gamma-toxin in the cornea. *Curr. Eye Res.* **42**, 1100–1107 (2017).
7. Dong, S. et al. Production and characterization of monoclonal antibody broadly recognizing cry1 toxins by use of designed polypeptide as hapten. *Anal. Chem.* **88**, 7023–7032 (2016).
8. Rasetti-Escargueil, C. & Popoff, R. M. Antibodies and vaccines against botulinum toxins: available measures and novel approaches. *Toxins* **11**, 528 (2019).
9. Chippaux, J.-P., Massougbodji, A., Diouf, A., Baldé, C. M. & Boyer, L. V. Snake bites and antivenom shortage in africa. *Lancet* **386**, 2252–2253 (2015).
10. Romo, J. A. et al. Development of anti-virulence approaches for candidiasis via a novel series of small-molecule inhibitors of candida albicans filamentation. *mBio* **8**, e01991–17 (2017).
11. Hoshino, Y. et al. The rational design of a synthetic polymer nanoparticle that neutralizes a toxic peptide in vivo. *Proc. Natl Acad. Sci. USA* **109**, 33–38 (2012).
12. Patke, S. et al. Design of monodisperse and well-defined polypeptide-based polyvalent inhibitors of anthrax toxin. *Angew. Chem. Int. Ed.* **53**, 8037–8040 (2014).
13. Hu, C.-M. J., Fang, R. H., Copp, J., Luk, B. T. & Zhang, L. A biomimetic nanosponge that absorbs pore-forming toxins. *Nat. Nanotechnol.* **8**, 336–340 (2013).
14. Chen, Y. et al. Broad-spectrum neutralization of pore-forming toxins with human erythrocyte membrane-coated nanosponges. *Adv. Healthc. Mater.* **7**, 1701366 (2018).
15. Walkinshaw, M. D., Saenger, W. & Maelicke, A. Three-dimensional structure of the "long" neurotoxin from cobra venom. *Proc. Natl Acad. Sci. USA* **77**, 2400–2404 (1980).
16. Gouaux, E., Hobaugh, M. & Song, L. alpha-Hemolysin, gamma-hemolysin, and leukocidin from *Staphylococcus aureus*: distant in sequence but similar in structure. *Protein sci.* **6**, 2631–2635 (1997).
17. Quintero-Hernández, V., Jiménez-Vargas, J. M., Gurrola, G. B., Valdivia, H. H. & Possani, L. D. Scorpion venom components that affect ion-channels function. *Toxicon* **76**, 328–342 (2013).

18. Pringos, E., Vignes, M., Martinez, J. & Rolland, V. Peptide neurotoxins that affect voltage-gated calcium channels: a close-up on ω-agatoxins. *Toxins* **3**, 17–42 (2011).
19. Naganawa, S. et al. Net positive charge of hiv-1 crf01_ae v3 sequence regulates viral sensitivity to humoral immunity. *PLoS ONE* **3**, e3206 (2008).
20. Bousarghin, L., Touzé, A., Combita-Rojas, A.-L. & Coursaget, P. Positively charged sequences of human papillomavirus type 16 capsid proteins are sufficient to mediate gene transfer into target cells via the heparan sulfate receptor. *J. Gen. Virol.* **84**, 157–164 (2003).
21. Butler, M., Medien, A. R. & Taylor, G. R. Electrofocusing of viruses and sensitivity to disinfection. *Water Sci. Technol.* **17**, 201–210 (1985).
22. Renner, C., Piehler, J. & Schrader, T. Arginine- and lysine-specific polymers for protein recognition and immobilization. *J. Am. Chem. Soc.* **128**, 620–628 (2006).
23. Sun, H., Lv, F., Liu, L. & Wang, S. Reactive conjugated polymers for the modulation of islet amyloid polypeptide assembly. *ACS Appl. Mater. Inter.* **11**, 22973–22978 (2019).
24. Sun, H. et al. Reactive amphiphilic conjugated polymers for inhibiting amyloid β assembly. *Angew. Chem. Int. Ed.* **58**, 5988–5993 (2019).
25. Poehler, E. et al. Label-free microfluidic free-flow isoelectric focusing, ph gradient sensing and near real-time isoelectric point determination of biomolecules and blood plasma fractions. *Analyst* **140**, 7496–7502 (2015).
26. Jin, Y., Luo, G., Oka, T. & Manabe, T. Estimation of isoelectric points of human plasma proteins employing capillary isoelectric focusing and peptide isoelectric point markers. *Electrophoresis* **23**, 3385–3391 (2002).
27. Abelha, T. F., Dreiss, C. A., Green, M. A. & Dailey, L. A. Conjugated polymers as nanoparticle probes for fluorescence and photoacoustic imaging. *J. Mater. Chem. B* **8**, 592–606 (2020).
28. Miao, Q. et al. Molecular afterglow imaging with bright, biodegradable polymer nanoparticles. *Nat. Biotechnol.* **35**, 1102–1110 (2017).
29. Wu, W., Bazan, G. C. & Liu, B. Conjugated-polymer-amplified sensing, imaging, and therapy. *Chem* **2**, 760–790 (2017).
30. Bhakdi, S. & Tranum-Jensen, J. Alpha-toxin of Staphylococcus aureus. *Microbiol. Rev.* **55**, 733–751 (1991).
31. Prévost, G. et al. Panton-valentine leucocidin and gamma-hemolysin from staphylococcus aureus atcc 49775 are encoded by distinct genetic loci and have different biological activities. *Infect. Immun.* **63**, 4121–4129 (1995).
32. Köster, S. et al. Crystal structure of listeriolysin o reveals molecular details of oligomerization and pore formation. *Nat. Commun.* **5**, 3690 (2014).
33. Moreno, M. & Giralt, E. Three valuable peptides from bee and wasp venoms for therapeutic and biotechnological use: melittin, apamin and mastoparan. *Toxins* **7**, 1126–1150 (2015).
34. Holaday, S. K., Martin, B. M., Fletcher, P. L. & Krishna, N. R. NMR solution structure of butantoxin. *Arch. Biochem. Biophys.* **379**, 18–27 (2000).
35. de Weille, J. R., Schweitz, H., Maes, P., Tartar, A. & Lazdunski, M. Calciseptine, a peptide isolated from black mamba venom, is a specific blocker of the l-type calcium channel. *Proc. Natl Acad. Sci. USA* **88**, 2437–2440 (1991).
36. Schweitz, H. et al. Calcicludine, a venom peptide of the kunitz-type protease inhibitor family, is a potent blocker of high-threshold ca^{2+} channels with a high affinity for l-type channels in cerebellar granule neurons. *Proc. Natl Acad. Sci. USA* **91**, 878–882 (1994).
37. Betzel, C. et al. The refined crystal structure of alpha-cobratoxin from naja naja siamensis at 2.4-a resolution. *J. Biol. Chem.* **266**, 21530–21536 (1991).
38. Scarselli, M. et al. NMR structure of alpha-bungarotoxin free and bound to a mimotope of the nicotinic acetylcholine receptor. *Biochemistry* **41**, 1457–1463 (2002).
39. Nicastro, G. et al. Solution structure of crotamine, a Na^{+} channel affecting toxin from crotalus durissus terrificus venom. *Eur. J. Biochem.* **270**, 1969–1979 (2003).
40. Dubovskii, P. V., Dementieva, D. V., Bocharov, E. V., Utkin, Y. N. & Arseniev, A. S. Membrane binding motif of the p-type cardiotoxin. *J. Mol. Biol.* **305**, 137–149 (2001).
41. Fajloun, Z. et al. Chemical synthesis and characterization of maurocalcine, a scorpion toxin that activates Ca^{2+} release channel/ryanodine receptors. *FEBS Lett.* **469**, 179–185 (2000).
42. Adams, D. J., Smith, A. B., Schroeder, C. I., Yasuda, T. & Lewis, R. J. ω-Conotoxin CVID inhibits a pharmacologically distinct voltage-sensitive calcium channel associated with transmitter release from preganglionic nerve terminals. *J. Biol. Chem.* **278**, 4057–4062 (2003).
43. Coulon, A. et al. Comparative membrane interaction study of viscotoxins a3, a2 and b from mistletoe (viscum album) and connections with their structures. *Biochem. J.* **374**, 71–78 (2003).
44. Floyd, R. & Sharp, D. Viral aggregation: effects of salts on the aggregation of poliovirus and reovirus at low pH. *Appl. Environ. Microbiol.* **35**, 1084–1094 (1978).
45. Kozlowski, L. P. IPC—isoelectric point calculator. *Biol. Direct* **11**, 55 (2016).